Robotic Precise Patch Clamp Measurement Method Based on a Tight and Stable Gigaseal

Jinyu Qiu, Bingxin Li, Ruimin Li, Yuzhu Liu, Xin Zhao, *Member, IEEE*, and Qili Zhao*, *Member, IEEE*

***Abstract*—The patch clamp technique has been widely utilized to measure extremely weak ion channel signals. In patch clamp technique, the measurement accuracy and duration rely on the tightness and stability of the seal between the aspirated cell membrane and the recording micropipette. The current patch clamp operations utilize a pressure-driven seal formation method that can only provide a 2D driving force on a small part of the aspirated cell membrane, which easily causes looseness or even failures of the seal, significantly limiting the measurement quality of ion channel signals. Addressing this, a robotic precise patch clamp measurement method was proposed in this paper. In this method, a 3D-driven seal formation method is developed to improve the measurement accuracy and duration of ion channel signals by providing a tight and stable gigaohm-scale seal (gigaseal). First, the forces applied by aspiration pressure and voltage on the aspirated cell membrane inside the micropipette are analyzed, respectively. Then, a dynamic model of the gigaseal formation process driven by pressure and voltage is established to provide a 3D driving force on the target aspirated cell membrane. Further, a dual-input adaptive sliding mode controller is developed to form a tight and stable gigaseal to improve the measurement accuracy and duration in patch clamp operation. Finally, a robotic precise patch clamp measurement process was established based on the above work. Experimental results on CA1 pyramidal neurons of mouse brain slices demonstrate that, in comparison to the current 2D-driven method, the proposed patch clamp measurement method has a 30% higher gigaseal formation success rate, 52% higher gigaseal resistance, and a fourfold increase in the success rate of 1-hour duration recordings, demonstrating the formation of a tighter and more stable gigaseal using our method. With the above advantages, a 3 dB-higher signal-to-noise ratio (SNR) was achieved, and long-term glycine-induced dynamic increases in amplitude and frequency of spontaneous excitatory postsynaptic currents (sEPSCs) were detected using the proposed method. With aforementioned higher measurement success rate, higher SNR and longer recording time, our patch clamp recording is expected to be applied in brain science and nervous system disease research in the future.**

***Index Terms*—Robotic patch clamp, gigaseal formation, electrophysiological recording, cell micromanipulation, 3D driving force, electroosmotic flow.**

I. Introduction

SINCE its invention by Neher and Sakmann in 1976 [1], the patch clamp technique has been widely recognized as the "gold standard" in cellular electrophysiology research due to its ability to measure the extremely weak ion channel signals of cells, which are usually at picoampere level (10^{-12} A) [2], [3]. As shown in Fig. 1, the patch clamp technique usually utilizes a microsized micropipette filled with conductive solution and inserted with an electrode wire to aspirate part of cell membrane into its opening to measure the ion channel signals. Before measurement, a gigaohm-scale seal (gigaseal) between the aspirated cell membrane and the inner surface of the micropipette should be formed first to shield the environmental electrical noise, enabling the detection of extremely weak ion channel signals. So, the measurement accuracy and duration of the ion channel signals in patch clamp are mainly determined by the tightness and stability of the gigaseal, respectively. Thereby, to achieve precise and long-time measurement of ion channel signals, a tight and stable gigaseal is required in patch clamp.

In conventional patch clamp operations [4], the operator empirically applies gentle suction pressure inside micropipette to aspirate part of cell membrane to form a gigaseal. As shown in Fig. 1, the cell membrane aspirated into micropipette usually has an Ω-shape. The aspiration pressure mainly generated pulling force on the free top surface of the aspirated cell membrane. The force being exered on the side surface of the aspirated membrane adhering to the inner wall of the micropipette is ignorable in comparison. Thus, only a 2D planar driving force is exerted on the top surface of the 3D Ω-shaped aspirated cell membrane during gigasealing formation process. When the above 2D driving force on free top surface is not balanced with the friction force between side surface and the inner wall of the mciropipette, it may cause the aspirated cell membrane to fold, tear or detach [5] from the inner wall of the micropipette during gigaseal formation porcess, which finally leads to looseness or even failures of the gigaseal. To form a tight and stable gigaseal, an extra driving force on the side surface of aspirated cell membrane is prefered to form a 3D whole driving force of the aspirated cell membrane, making the aspirated cell membrane in a balanced state to creep smoothly along the inner wall of the micropipette to form a high quality gigaseal.

In recent years, numerous approaches have been reported to improve the tightness and stability of gigaseal. Since the tightness and stability of the gigaseal are positively correlated with the adhesion between the cell membrane and the inner surface of the micropipette, these efforts mainly focus on enhancing the adhesion. For example, adding reducing agents [6] or changing the ionic composition [7] in the bath solution

This research was jointly supported by National Natural Science Foundation of China (62273186), Guangdong Basic and Applied Basic Research Foundation (2024A1515011171) and Tianjin Science and Technology Major Project under the grant (No.24ZXZSSS00420).

Jinyu Qiu, Bingxin Li, Ruimin Li, Yuzhu Liu, Xin Zhao and Qili Zhao are with the Institute of Robotics and Automatic Information System (IRAIS), the Tianjin Key Laboratory of Intelligent Robotic (tjKLIR), Nankai University, Tianjin 300350, China, the Engineering Research Center of Trusted Behavior Intelligence, Ministry of Education, Nankai University, Tianjin 300350, China, the National Key Laboratory of Intelligent Tracking and Forecasting for Infectious Diseases, Nankai University, Tianjin 300350, China, the Institute of Intelligence Technology and Robotic Systems, Shenzhen Research Institute of Nankai University, Shenzhen 518083, China.

*Corresponding author: Qili Zhao. (e-mail: zhaoqili@nankai.edu.cn)

This article has been accepted for publication in IEEE Transactions on Instrumentation and Measurement. This is the author's version which has not been fully edited and content may change prior to final publication. Citation information: DOI 10.1109/TIM.2025.3635816

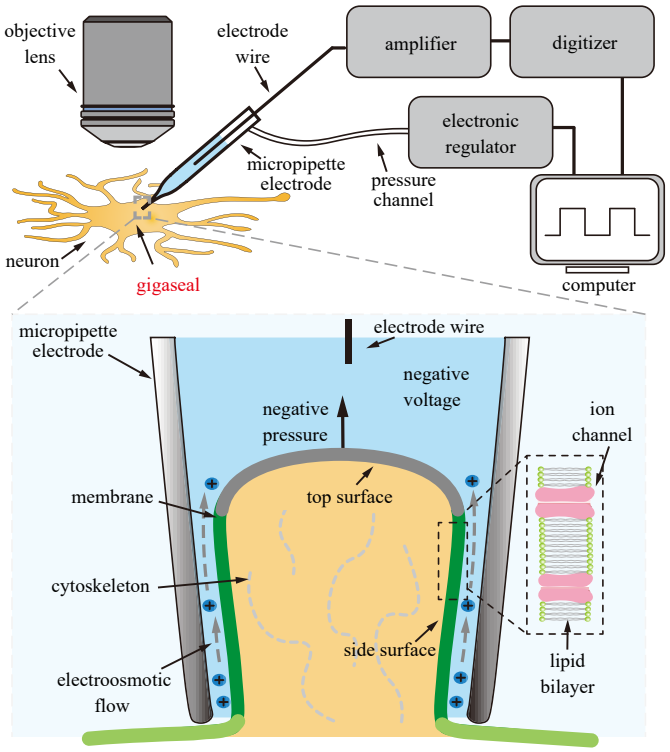

Fig. 1. The schematic diagram of gigaseal formation in patch clamp operation.

has been shown to enhance the adhesion between the cell membrane and glass surface by modifying the properties of the cell membrane surface. However, the effects of reducing agents and ions on biological systems limit these methods to being used only for specific ion channel studies. Fire polishing of the micropipette [8] or modifying the hydrophilicity of its surface through chemical methods [9] have also been reported to improve the adhesion of the cell membrane. However, since the micropipette is usually single-use for each recording, these methods for micropipette treatment significantly increase the cost and complexity of the recordings. Moreover, the above methods enhance the tightness of the gigaseal by modifying the surface properties of the cell membrane or the micropipette, but they do not consider the effect of the gigaseal driving process on the tightness and stability of the seal.

In recent years, research on robotic patch clamp systems has made significant progresses due to the rapid development of computer technologies and robotics. However, according to the best of our knowledge, few of them have made significant improvements in the quality of the gigaseal. For example, the planar patch clamp system uses a microhole array connected with a pump to aspirate multiple floating cells and measure them at one time automatically [10]. However, the hole-in-plane structure makes it hard to form a tight and stable gigaseal, which makes the final sealing impedance in the plane patch clamp usually smaller than that of conventional patch clamp system. Besides, the hole-in-plane structure makes the plane patch clamp system not suitable for adherent cells or cells in vivo. The blind patch clamp systems utilize the measured impedance of the micropipette electrode to conduct patch clamp operation on adherent cells and even cells in vivo automatically without visual feedback [11]. However, a lack of visual guidance usually leads to lower success rates of gigaseal formation in comparison to conventional patch clamp systems. As improvements, differential interference contrast (DIC) imaging [12] and two-photon microscopy imaging [13] which are able to depict label-free neurons in brain slices and the fluorescence dye-labeled neurons in live animal brains, respectively, have been utilized to conduct robotic patch clamp on these cell types. Specially, we previously developed a robotic patch clamp system utilizing the measured 3D cell morphology to select an appropriate contact point on cell surface to perform gigaseal formation [14] thereby improving the success rate of gigaseal formation. In addition, we designed a robotic stepwise micropipette navigation process [15] that nearly doubled the operation speed of the micropipette from its initial position to the target neuron surface. The previously reported automated methods and our own previous work have all focused on the micropipette navigation step of the patch clamp operation. However, in the essential gigaseal formation step, they still relied on empirically preset pressures [10]–[14] or only provided a 2D driving force that mimic manual operation [15], thereby limiting improvements in gigaseal tightness and stability. Therefore, a new robotic gigaseal formation method is still desired to improve the tightness and stability of gigaseal, and thereby, increase the recording accuracy and duration of the patch clamp.

As mentioned before, to facilitate the formation of a tight and stable gigaseal, an extra driving force is preferred to be generated on the side surface of the aspirated membrane to form a 3D driving force combined with aspiration pressure. The creeping of the aspirated cell membrane along the glass surface of the micropipette has been observed to be voltage-sensitive by Gil et al. [16]. Suchyna et al. [5] further found that applying positive and negative voltages to the micropipette can respectively promote and inhibit the creeping of the membrane patch along the micropipette in suitable solutions. They attributed this effect to electroosmosis caused by the charges present on both the membrane and the glass. Therefore, the voltage applied to the micropipette can induce electroosmotic forces on the side surface of the aspirated cell membrane adhering to micropipette. Compared to pressure-induced force which only acts concentrately on the free top surface membrane (see Fig. 1), the electroosmotic force is more precise and uniformly distributed at the side surface of aspirated membrane. Thus, it may be utilized in conjunction with pressure to provide a 3D force to drive the aspirated cell membrane to smoothly creep along inner wall of micropipette, finally forming a tight and stable gigaseal.

In this paper, a robotic precise patch clamp measurement method was realized based on a tight and stable gigaseal. A novel 3D-driven gigaseal formation method is developed to improve the tightness and stability of gigaseal, and thereby increase the accuracy and duration of patch clamp measurement method. First, the forces applied by aspiration pressure and voltage on the aspirated cell membrane inside the micropipette are analyzed, respectively. Then, a dynamic model of the gigaseal formation process driven by pressure and voltage

is established to provide a 3D driving force on the target aspirated cell membrane. Further, a dual-input adaptive sliding mode controller is developed to form a tight and stable gigaseal to improve the measurement accuracy and duration in patch clamp operation. Finally, a robotic precise patch clamp measurement process is established based on the above work. The robotic whole-cell patch clamp experiments on 20 CA1 pyramidal neurons of mouse brain slices demonstrate that in comparison to the conventional 2D-driven method and the reported automated gigaseal methods, the proposed patch clamp measurement method has a significantly higher success rate in gigaseal formation (85% vs. 55% and 60%, n=20) and higher final seal resistance (3.09±0.58 GΩ (n=17) vs. 2.03±0.62 GΩ (n=11) and 2.13±0.56 GΩ (n=12)). Further, a fourfold increase in the number of successful long-time (longer than one hour) measurement of ion channel signals was achieved in comparison to both the conventional method and the reported automated method (8 vs. 2 and 2 successful 1-hour recordings in 20 trials), proving the improved stability of the gigaseal formed using our method. Potentially attributed to the above tighter and more stable seal, our method achieves a 3 dB higher signal-to-noise ratio (SNR) (12 dB vs. 9 dB) in the measurement of spontaneous excitatory postsynaptic currents (sEPSCs) in comparison to the above two methods. Additionally, action potentials and sEPSCs of the target neurons measured using the proposed method prove no significant negative influence on electrophysiological activities of operated cell using our method. Besides, a 32% dynamic increase in amplitude and a 132% dynamic increase in frequency were observed in sEPSC recordings using our method after 60 minutes of glycine treatment. The results prove the effectiveness of our robotic patch clamp measurement method in investigating the long-term variations of electrophysiological activities of neurons induced by drugs, which is of great meaning in the study of pathological and pathogenic mechanisms of neuron system diseases and their potential treatment research. With the above advantages, our method is highly expected to be applied in brain science and nervous system disease research.

II. System Setup

The precise patch clamp measurement method was performed using the robotic patch clamp system developed within our laboratory [14]. As shown in Fig. 2, an immovable stage mounted on a vibration-isolation table is utilized to position the storage chamber containing brain slices. A standard upright microscope (Eclipse FN1, Nikon) mounted on the motor stage capable of moving in X-Y plane (with a travel range of 50 mm×50 mm, a maximum speed of 1 mm/s, and repeatability of ±0.1 μm; MP285, Sutter Instrument) is utilized to observe the neurons. A CCD camera (IR-2000, DAGE-MTI) is mounted on the microscope to acquire images at 60 fps. A motorized focus device (with a repeatability of ±0.1 μm; ES10ZE, Prior) is installed on the microscope to position the focal plane. An X-Y-Z micromanipulator (with a working space of 50 mm×50 mm×50 mm, a maximum speed of 1 mm/s, and repeatability of ±0.1 μm; MP285, Sutter Instrument) is used to position the micropipette. A signal

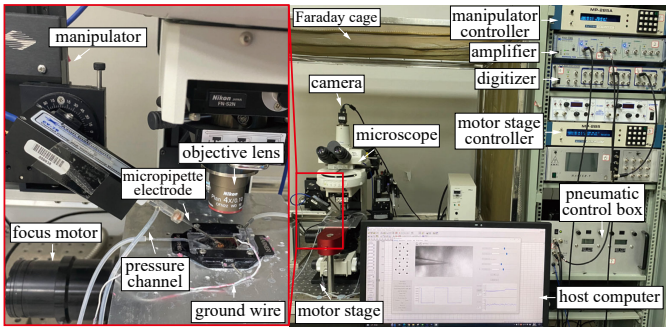

Fig. 2. Robotic patch clamp system setup.

amplifier (Multiclamp 700B, Axon Instruments) and a data acquisition device (DAQ USB-6211, National Instruments) are used for voltage control and signal acquisition, respectively. An in-house developed pneumatic control box provides an aspiration pressure with a range from −5 psi to 15 psi and a resolution of 10 Pa. The custom-developed human-machine interface (HMI), written in C++, controls all the aforementioned hardware in a multi-threaded manner. The HMI allows the operator to monitor the system state in real-time, such as resistance values, pressure values, manipulator positions, imaging, and error warnings, etc. It also supports manual intervention during automated patch clamp processes when necessary.

The preparation of mouse brain slices and micropipettes can be found in the "Materials Preparation" section of the "Supplemental file.docx". All experimental procedures involving mice were approved by the Committee for Animal Experimentation of the College of Life Sciences at Nankai University (No. 2008) and were performed in accordance with the NIH Guidelines for the Care and Use of Laboratory Animals (No. 8023, revised in 1996).

III. Key Methodologies and Technologies

To achieve a smoother and more controllable gigaseal formation process for tight and stable gigaseal, the driving forces of aspiration pressure and voltage in gigaseal formation are modeled, respectively. Then a dynamic model of gigaseal formation process under the combined 3D driving force provided by pressure and voltage is established. Based on the above work, a dual-input adaptive sliding mode controller is designed to control the gigaseal formation process along the designed smooth sealing resistance trajectory.

A. Pressure-Induced Force Modeling in Gigaseal Formation

The force induced by the pressure on the cell membrane aspirated into micropipette is analyzed in this section.

First, the geometry of the micropipette tip in the gigaseal formation region is reasonably simplified to facilitate the following analysis. Although the tip of the micropipette is typically conical due to the pulling process, it is often post-polished [8], [17] to smooth the tip for improving sealing process, which reduces the variation of inner diameter of the tip. Since the gigaseal only forms at the very tip of

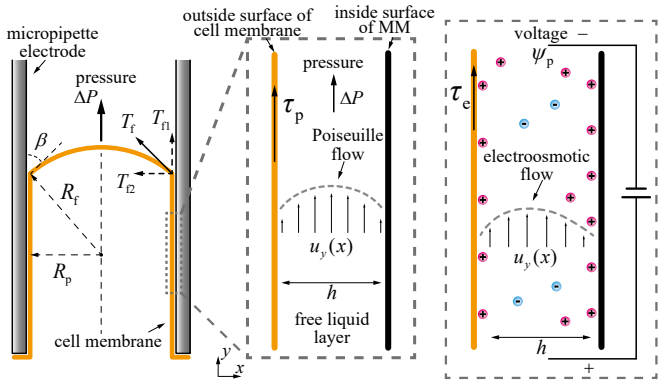

Fig. 3. The gigaseal formation model driven by aspiration pressure and voltage.

the micropipette, where the variation in diameter is relatively small, the inner diameter of the micropipette tip is modeled as a constant in the following analysis.

The aspirated cell membrane usually has Ω-shape under high resolution microscopy [18] (see Fig. 3). The portion of the cell membrane adheres to micropipette (side surface) due to the lipid-glass adhesion interaction (caused by hydrogen bonds, van der Waals forces, etc. [19]). The remaining portion of the membrane not in contact with the inner wall of micropipette (top surface) forms a freestanding dome under the aspiration pressure.

Strictly speaking, when the pressure ΔP is applied inside the micropipette, the resulting force on the aspirated cell membrane comprises two components: the force directly acting on the freestanding top surface and the force acts on the adhered side surface exerted by the pressure induced flow. The above two forces are analyzed and compared as follows.

1) The force directly acting on the top surface: Considering that the volume of the aspirated membrane patch is only at the cubic micron scale, containing a limited amount of proteins and cytoskeleton, their effects are neglected in the following analysis. Under these conditions, an ideal freestanding membrane with a radius of curvature R_f satisfies the Laplace law [18], [20]

$$T_f = \frac{\Delta P R_f}{2} \tag{1}$$

where T_f is the surface tension of the freestanding membrane, indicating the force per unit length, R_f is the radius of curvature of the freestanding membrane. At the interface between the freestanding and adhered membrane (see Fig. 3), T_{f2} is the component of T_f perpendicular to the surface of the micropipette, which balances with the maximum line adhesion tension between the membrane and the micropipette. Meanwhile, T_{f1} is the component of T_f parallel to the surface of the micropipette, which is the source of the force that pulls the cell membrane to creep along the micropipette. According to (1) and the geometric relationships, T_{f1} can be calculated as

$$T_{f1} = T_f \cos\beta = \frac{\Delta P R_f}{2}\frac{R_p}{R_f} = \frac{\Delta P R_p}{2} \tag{2}$$

where β is the contact angle between the membrane and the inner surface of the micropipette, and R_p is the inner radius of the micropipette. Thus, the force directly acting on the membrane which pulls the cell membrane can be calculated as

$$F_p = 2\pi R_p T_{f1} = \pi {R_p}^2 \Delta P \tag{3}$$

2) The force exerted by the pressure induced flow on side surface: Assuming that the adhesion structure between the aspirated cell membrane and the glass is flat common black films [21], which contain a free liquid layer with a thickness of about 10 nm between a hydrophilic lipid layer and a glass surface (see Fig. 3). When the pressure ΔP is applied across this liquid layer, it induces a parabolic Poiseuille flow of low-Reynolds number [19]:

$$u_y(x) = \frac{1}{2\eta}\frac{\Delta P}{L}x(h-x) \tag{4}$$

where $u_y(x)$ is the velocity of the laminar flow in the direction of y, with a velocity distribution along the x-axis, η is the kinematic viscosity of the liquid, L is the length of the adhered membrane, and h is the thickness of the liquid layer. According to Newton's law of viscosity, the force exerted by this flow on the membrane surface can be obtained as

$$F_s = \tau_p \cdot S = -\eta \frac{du_y}{dx}\bigg|_{x=0} \cdot 2\pi R_p L = \pi R_p h \Delta P \tag{5}$$

where S is the area of the adhered cell membrane, τ_p is the shear stress exerted by the flow on the side surface, indicating the force per unit area in the direction of y.

The thickness of the liquid layer h (approximately 10 nm) is much smaller than the inner radius of R_p (approximately $1-2$ μm), which means $F_s \ll F_p$ according to (3) and (5). Therefore, in the two components of the pressure's effect on the cell membrane, the force exerted by the pressure induced flow within the liquid layer can be ignored. Thus, the force induced by pressure mainly acts on the top surface of the aspirated membrane, providing a 2D driving force.

B. Voltage-Induced Force Modeling in Gigaseal Formation

Due to the relatively negative potential inside the cell compared to the outside during the resting phase, the outside of the cell membrane is positively charged [19]. Additionally, in standard aCSF (Artificial Cerebrospinal Fluid) with a pH = 7.4, the micropipette surface shows cation adsorption due to chemical reactions between glass and ions, resulting in positive charges on its surface as well [22]. In the adhesion structure between the aspirated membrane and the inner surface of the glass micropipette in Section III(A), when a potential is applied across the liquid layer, it satisfies the conditions required for electroosmotic flow: an electric double layer, electrolyte solution, an applied electric field across a channel of suitable dimensions [22], [23]. The net charge in the solution, generated by the aforementioned electric double layers, will move due to the Coulomb force induced by the electric field, resulting in electroosmotic flow (see Fig. 3).

In the electroosmotic flow under an applied potential ψ_{p} with low-Reynolds number, the balance between viscous friction and Coulomb force satisfies the Navier-Stokes equation

$$\eta \frac{d^2 u_y}{dx^2} + \rho_e E_y = 0 \tag{6}$$

where $E_y = -\psi_{\mathrm{p}}/L$ is the electric field in the direction of y, ρ_e is net-charge density in the solution, which is described by the Poisson-Boltzmann equation [22]

$$\nabla^2 \psi = -\frac{\rho_e}{\varepsilon_0 \varepsilon_{\mathrm{r}}} = -\frac{\sum \alpha_i e_0 C_{i\infty} \exp(-\alpha_i e \psi / k_{\mathrm{B}} T)}{\varepsilon_0 \varepsilon_{\mathrm{r}}} \tag{7}$$

where ψ is the electric potential distributed along the x-axis, ε_0 is vacuum electrical permittivity (ε_0=8.854$\times 10^{-12}$F/m), ε_{r} is the relative permittivity with respect to vacuum of the solution, e_0 is the electron charge, α_i and $C_{i\infty}$ are the valence and the bulk concentration of type ith ion respectively, k_{B} is the Boltzmann constant (k_{B}=1.380649 $\times 10^{-23}$J/K), and T is the absolute temperature of the solution.

Substituting (7) into (6) obtains

$$\eta \frac{d^2 u_y}{dx^2} - \varepsilon_0 \varepsilon_{\mathrm{r}} E_y \frac{d^2 \psi}{dx^2} = 0 \tag{8}$$

Integrating equation (8) twice obtains (9) and (10), respectively.

$$\eta \frac{du_y}{dx} - \varepsilon_0 \varepsilon_{\mathrm{r}} E_y \frac{d\psi}{dx} = k_1 \tag{9}$$

$$\eta u_y(x) - \varepsilon_0 \varepsilon_{\mathrm{r}} E_y \psi(x) = k_0 + k_1 x \tag{10}$$

According to the boundary conditions, the fluid velocity $u_y(x)$ at both the top and bottom walls is zero, which means $u_y(0) = u_y(h) = 0$. Substituting these boundary conditions into (10) obtains

$$k_1 = \varepsilon_0 \varepsilon_{\mathrm{r}} E_y \frac{\psi(0) - \psi(h)}{h} \tag{11}$$

Substituting (11) into (9), and according to Newton's law of viscosity, the shear stress τ_{e}, which represents the force per unit area in the direction of y exerted by the electroosmotic flow on the cell membrane, is obtained by

$$\tau_{\mathrm{e}} = \eta \left.\frac{du_y}{dx}\right|_{x=0} = -\varepsilon_0 \varepsilon_{\mathrm{r}} \left(\frac{\psi(0) - \psi(h)}{h} + \psi'(0)\right) \frac{\psi_{\mathrm{p}}}{L} \tag{12}$$

where the surface potential $\psi(0)$ of the membrane, the surface potential $\psi(h)$ of the micropipette and the potential gradient $\psi'(0)$ are determined by the cellular state, the composition and the pH of the solution.

Consequently, the force induced by the voltage ψ_{p} on the side surface of aspirated cell membrane is

$$F_{\mathrm{v}} = \tau_{\mathrm{e}} \cdot S = -2\pi R_{\mathrm{p}} \varepsilon_0 \varepsilon_{\mathrm{r}} \left(\frac{\psi(0) - \psi(h)}{h} + \psi'(0)\right) \psi_{\mathrm{p}} \tag{13}$$

After the gigaseal is established, applying voltage to the micropipette changes the potential difference between the inside and outside of the membrane. The potential difference exceeding the threshold may activate some voltage-gated ion channels on the membrane. Therefore, the voltage is applied only before the gigaseal is established and is subject to the constraint $\psi_{\mathrm{c}} \le \psi_{\mathrm{p}} \le 0\mathrm{mV}$, where ψ_{c} is the lower constraint of the applied voltage.

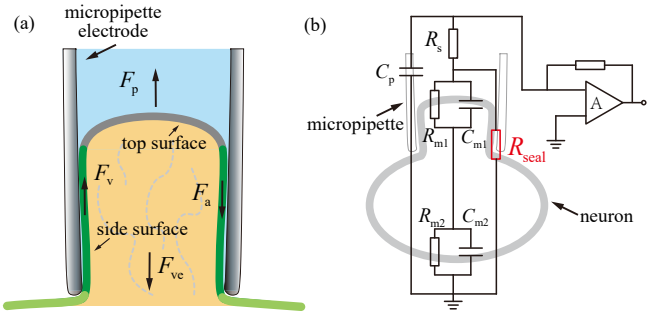

Fig. 4. Force analysis and electrical model of gigaseal formation. (a) The main forces involved in gigaseal formation. Forces generated by the pressure and voltage is represented by F_{p} and F_{v}, respectively. The adhesive force between the membrane and the micropipette is represented by F_{a}. The viscoelastic force of the cell is represented by F_{ve}. (b) The electrical model of gigaseal formation. The distributed resistance at the membrane-glass adhesion region is represented by R_{seal}. The cell membrane inside the micropipette is modeled as a parallel resistance-capacitance circuit, represented by R_{m1} and C_{m1}, while the cell membrane outside the micropipette is modeled by R_{m2} and C_{m2}. The series resistance between the amplifier and the micropipette is represented by R_{s}. The capacitance of the micropipette glass wall is represented by C_{p}.

C. The Dynamic Model of Gigaseal Formation Process Under Combined 3D Driving Forces of Pressure and Voltage

According to the viscoelastic properties of the cell described by the Kelvin-Voigt model [24], the cell membrane being drawn into the micropipette is subjected to the cell's viscoelastic forces F_{ve}. Additionally, as shown in Fig. 4(a), under the combined action of pressure and voltage, the cell membrane aspirated inside the micropipette is subjected to the 3D forces generated by the pressure and voltage, as well as the frictional force F_{a} due to adhesion between membrane and glass interaction. Consequently, the resultant force on the cell membrane within the micropipette is obtained as

$$F = F_{\mathrm{p}} + F_{\mathrm{v}} - \mu_{\mathrm{a}} 2\pi R_{\mathrm{p}} L - k_{\mathrm{e}} L - k_{\mathrm{v}} \dot{L} \tag{14}$$

where μ_{a} is the frictional force per unit area of the adhered cell membrane [25], which is assumed here to be constant under small velocity variations, k_{e} and k_{v} are the elastic and viscous coefficients of the cell, respectively.

Substituting (3) and (13) into (14), and according to Newton's law, the dynamic model of the aspirated cell membrane in the micropipette is

$$\begin{aligned} F =& m\ddot{L} \\ =& \pi {R_{\mathrm{p}}}^2 \Delta P + 2\pi R_{\mathrm{p}} \varepsilon_0 \varepsilon_{\mathrm{r}} \left(\frac{\psi(0) - \psi(h)}{h} + \psi'(0)\right)(-\psi_{\mathrm{p}}) \\ & - \mu_{\mathrm{a}} 2\pi R_{\mathrm{p}} L - k_{\mathrm{e}} L - k_{\mathrm{v}} \dot{L} \end{aligned} \tag{15}$$

where m is the mass of the cell membrane in the micropipette.

In patch clamp experiments, due to the interior of the tilting micropipette is usually invisible, the length L of the aspirated cell membrane in the micropipette is hard to be measured by imaging. Addressing this, an electrical model of gigaseal is established as shown in Fig. 4(b). Due to the high resistance R_{m1} and R_{m2} of the membrane lipid bilayer [26] and the small series resistance R_{s} in the circuit, the measured resistance R

is approximately equal to the resistance R_{seal} of the adhered region, which is commonly used to assess the condition of the seal as feedback. The adhered region has been demonstrated to have distributed resistance [1], assuming that this resistance is uniformly distributed across it, and given that $h \ll R_{\mathrm{p}}$, the relationship between the membrane length L and the measured resistance R is expressed as

$$L = \frac{R}{\rho} 2\pi R_{\mathrm{p}} h \tag{16}$$

where ρ is the electrical resistivity of the seal media [3]. Let $x = L$, $u_1 = \Delta P$, $u_2 = -\psi_{\mathrm{p}}$, $a = -\frac{k_{\mathrm{v}}}{m}$, $b = -\frac{\mu_{\mathrm{a}} 2\pi R_{\mathrm{p}} + k_{\mathrm{e}}}{m}$, $c = \frac{\pi {R_{\mathrm{p}}}^2}{m}$, and $d = \frac{2\pi R_{\mathrm{p}} \varepsilon_0 \varepsilon_{\mathrm{r}}}{m} (\frac{\psi(0) - \psi(h)}{h} + \psi'(0))$. Under experimental conditions, c and d are both positive. Equation (15) can be rewritten as

$$\ddot{x} = a\dot{x} + bx + cu_1 + du_2 + f(t) \tag{17}$$

where $f(t)$ is a function of both the unknown internal dynamics (including the dynamic changes of membrane proteins, cytoskeleton, etc.) and the external disturbance. It is assumed that the disturbance is uniformly bounded and there exists positive constants δ_1 and δ_2 that $|f(t)| \leq c\delta_1 + d\delta_2$.

In the model represented by equation (17), some parameters are uncertain and dynamic in experiments, making them difficult to be precisely measured. The above parameters include the mass of the cell membrane in the micropipette, the potential distribution in the liquid layer between the adhered membrane and the glass, and the viscoelastic coefficients of the cell. Addressing this, a dual-input adaptive sliding mode controller (ASMC) is designed to facilitate the gigaseal formation under the combined inputs of pressure and voltage in the presence of various parameter uncertainties. Details of the controller design and the stability proof are provided in the "Controller Design for 3D-Driven Gigaseal Formation" section, while the simulation results, including a comparison between the single-input PID controller using pressure only (SI-PID) and the dual-input PID controller using both pressure and voltage inputs, are presented in the "Simulation of Dual-Input ASMC" section of the "Supplemental file.docx".

D. Robotic Precise Patch Clamp Measurement Process Based on 3D-driven Gigaseal Formation

A robotic precise whole-cell patch clamp measurement process based on 3D-driven gigaseal formation method is established as shown in Fig. 5(a). First, the micropipette is automatically lowered until a circuit current is detected, indicating that the tip enters the extracellular solution. When the micropipette tip is bathed in the solution, a low positive pressure of 0.5 psi is applied inside the micropipette to generate a fine flow out of the micropipette opening, reducing clogging issues. The objective lens is then lowered to focus the micropipette tip into view and move it to the image center using image processing [27]. Further, the system lowers the objective lens and micropipette simultaneously until the neurons on the surface of the brain slice are in focus. During this process, the micropipette tip is kept at 50 μm above the focal plane to avoid touching the tissue. After the target neuron is selected by mouse clicking, the micropipette approaches the cell surface from above based on the calculated relative position between the cell and the micropipette tip. During the process, the resistance is monitored in real time. When the resistance rises to a threshold (set in the experiments to be 0.5 MΩ higher than the bath resistance), the opening of the micropipette is considered to be covered by the cell membrane. Details of the robotic micropipette navigation process before gigaseal formation can be found in the "Robotic Micropipette Navigation Process" section of the "Supplemental file.docx".

Then the dual-input ASMC begins to operate, increasing the seal resistance along the desired trajectory, which is determined through forces analysis of the gigaseal formation process and experimental experience from more than 500 gigaseal formation trials. During gigaseal formation, the cell membrane inside the micropipette is mainly subjected to the following forces: viscoelastic forces F_{ve} of the membrane, the adhesion force F_{a} between the adhered membrane and the micropipette, and the forces F_{p} and F_{v} applied by pressure and voltage, respectively. Analysis of numerous experiments indicates that the membrane aspiration process can be divided into three phases: (i) In the starting stage, only a small portion of the membrane is aspirated into the micropipette tip, and the adhesion force is weak. To prevent detachment, rapid aspiration is required, so the seal resistance needs to increase rapidly. (ii) In the middle stage, the membrane creeps along the inner wall of the micropipette. To ensure smooth gigaseal formation, the seal resistance should increase at a constant rate. (iii) In the ending stage, once the seal resistance reaches the GΩ level, a sufficient length of membrane has been aspirated into the micropipette. To avoid overstretching and potential damage of the membrane, the applied pressure and voltage are stopped. At this stage, the adhesion force is large enough to maintain membrane attachment to the micropipette wall, allowing the seal resistance to gradually stabilizes. Based on the above force analysis and experimental observations, the desired trajectory is set as a function which initially increases with a constant acceleration of a_{L}, then continues to rise at a constant velocity v_{L} until the resistance reaches gigaohm-scale (see the desired trajectory in Fig. 6). Subsequently, when the seal resistance reaches GΩ level, the pressure and voltage inputs are stopped to prevent the cell membrane from being damaged due to excessive stretching. The seal structure then gradually stabilizes under the influence of forces such as membrane-glass adhesion. When the absolute value of the resistance variation rate remains below 10 MΩ per second for more than 30 seconds, the gigaseal is considered to be stable and considered as the final seal resistance. The parameters of the desired trajectory were further refined using resistance trajectory data recorded from experienced operators. The parameters of the model and the desired trajectory set are listed in Table I.

Then, negative pressure pulses with an amplitude of -5 psi and a duration of 1 s determined through previous research [28] are repeatedly applied inside the micropipette to break the membrane patch at the micropipette tip, thereby establishing a whole-cell configuration for signal recordings. It is considered a successful whole-cell recording in this system if

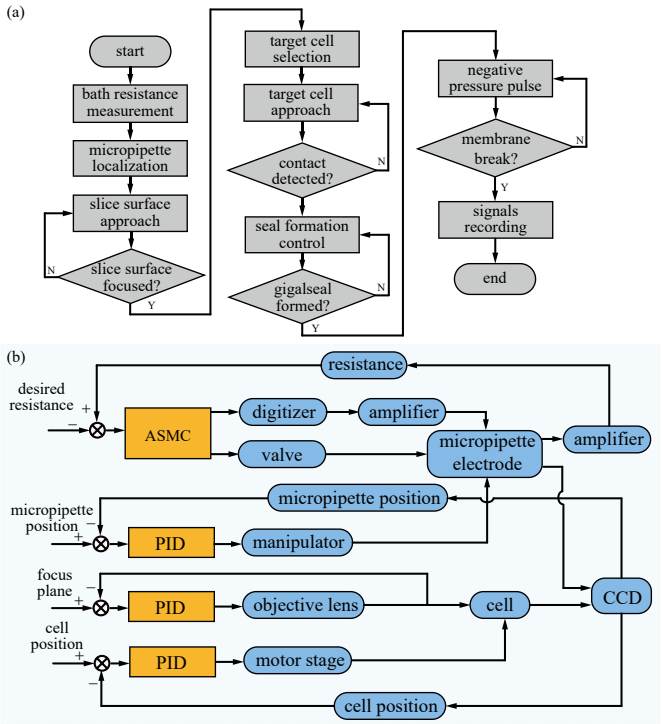

Fig. 5. The robotic patch clamp process based on 3D-driven gigaseal formation method. (a) The flow chart of the robotic patch clamp process. (b) The control diagram of the robotic patch clamp system.

TABLE I
PARAMETERS OF THE MODEL

symbol	value	symbol	value
R_{p}	1 μm	$\psi(0)$	60 mV
m	1.017×10^{-11} g	$\psi(h)$	30 mV
k_{e}	1.3×10^{-3} N/m	$\psi'(0)$	30 mV/nm
k_{v}	9.6×10^{-3} kg/s	ψ_{c}	−70 mV
μ_{a}	600 N/m^2	ρ	0.85 Ωm
ε_{r}	80	a_{L}	4 MΩ/s^2
h	1 nm	v_{L}	52 MΩ/s

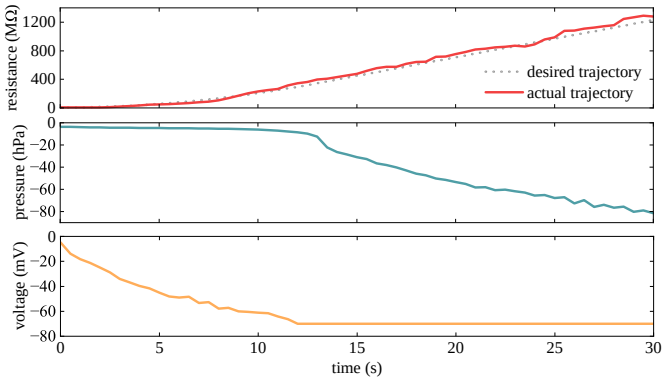

Fig. 6. Time course of the desired resistance, the measured resistance, the applied pressure, and the applied voltage during the gigaseal formation process using the proposed method.

the resistance decreases to less than 500 MΩ within 5 pulses (set based on the protocol described in [28]). Spontaneous excitatory postsynaptic currents (sEPSCs) are then recorded with the membrane potential clamped at −70 mV.

During the above robotic patch clamp process, the PID controllers are designed to control the motion of the micropipette, microscope and focus device. The control diagram of the robotic patch clamp system is shown in Fig. 5(b). Details of the control diagram can be found in the "Control Diagram of the Robotic Patch Clamp System" section of the "Supplemental file.docx". The above robotic patch clamp process is shown in the "Robotic Precise Patch Clamp Recording Process.mp4".

IV. Experimental Results

A total of 60 healthy CA1 pyramidal neurons were randomly selected from 20 brain slices (3 neurons for each slice) obtained from 10 four-week-old mice (2 slices for each mice). These neurons were randomly divided into three groups, each containing 20 neurons. The first group was operated manually by an operator with one year of patch clamp experience using the conventional method, in which negative pressure was generated with the piston of a 1 mL syringe to aspirate the cell membrane [4], [8]. The second group was performed on our system using the reported automated method [12], with an empirically preset small negative pressure ranging from −0.2 to −1.0 psi applied during gigaseal formation process through a pneumatic control box. The third group was performed using the method proposed in this paper.

First, gigaseal formation experiments were conducted to compare the success rate and quality of gigaseal formation using the above three methods. The number of successful gigaseal and the final seal resistance were compared to evaluate the tightness of gigaseal. Then, electrophysiological signal recording experiments were conducted to compare the success rate, SNR and duration of signal recording achieved by the above three methods. The number of successful whole-cell recordings, the SNR of the recorded sEPSCs, and the number of successful 60-minute recordings were compared. Finally, in order to validate the advantages of the high-quality long-time recordings achieved by the proposed methods in neuroscience research, long-time glycine-induced sEPSCs in the CA1 region were recorded and analyzed.

A. Gigaseal Formation Experiments

The success rate of gigaseal formation critically impacts the efficiency of patch clamp recordings. In the experiments, a final seal resistance reaching the gigaohm-scale was considered a successful gigaseal formation. The time course of the desired resistance, the measured resistance, the applied pressure, and the applied voltage during a gigaseal formation process using the gigaseal formation control method is shown in Fig. 6. The average root mean square error (RMSE) of tracking errors for the desired resistance trajectory is only 58.85 MΩ (n=17), which is less than 1.9% of the final seal resistance, indicating that our method achieved a smooth gigaseal formation process. As shown in Fig. 7(a), the conventional method, the reported automated method, and the proposed method achieve gigaseal formation success rates of 55% (11/20), 60% (12/20), and 85% (17/20), respectively. The superior success rate of the proposed method over the other two methods demonstrates that

the proposed gigaseal formation control method significantly enhances the success rate of gigaseal formation.

After achieving a gigaohm-scale seal resistance, the pressure and voltage inputs were stopped. The final seal resistances described in Section III(D) of three groups were compared. The experimental results shown in Fig. 7(b) demonstrate that the conventional method, the reported automated method, and the proposed method achieved final seal resistances of 2.03±0.62 GΩ (n=11), 2.13±0.56 GΩ (n=12), and 3.09±0.58 GΩ (n=17), respectively. The final seal resistance achieved by the proposed method is statistically significant higher compared to the conventional method (with ***p=0.00009) and the reported automated method (with ***p=0.0001). As the final seal resistance of gigaseal is positively correlated with the adhesion tightness between the cell membrane and the inner wall of the micropipette, the higher seal resistance achieved by the proposed method indicates that our method forms tighter gigaseals. The higher tightness of the seal is likely attributable to the 3D driving force instead of 2D driving force, and the smooth creeping of the cell membrane achieved by our method during gigaseal formation process, which enhances its adhesion to the inner wall of the micropipette. The higher final seal resistance is beneficial for the stability of the gigaseal structure and the SNR in subsequent signal recordings.

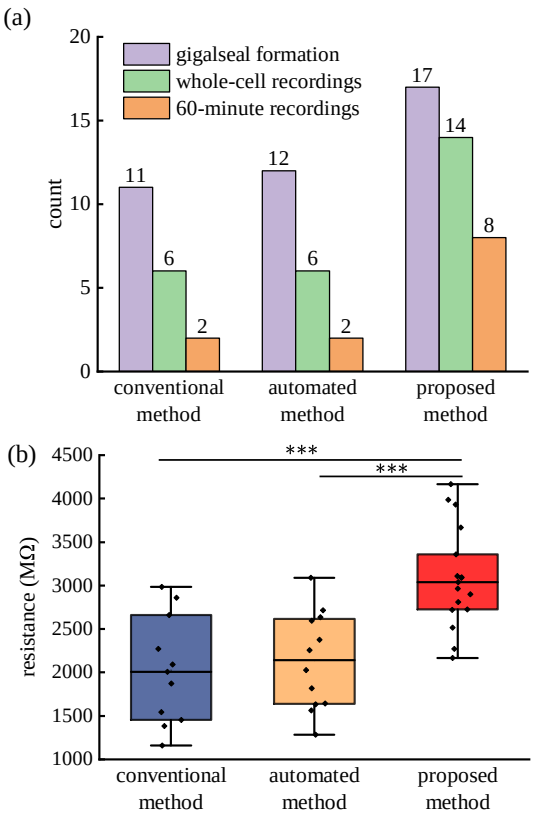

Fig. 7. Experimental results of the conventional method, the reported automated method, and the proposed method. (a) The number of successful gigaseal formation, whole-cell recordings, and 1-hour recordings for each group, with each group consisting of 20 trials. (b) The final seal resistances.

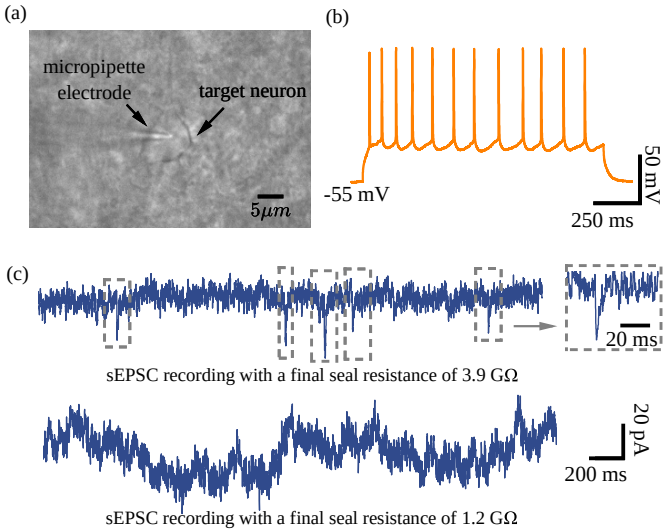

Fig. 8. Signal recordings of patch clamp whole-cell configuration after the operation of the proposed method. (a) The micropipette and the target neuron during the recording. (b) Action potentials recorded from the target neuron with a 1000 ms-long current injection pulse at 100 pA. (c) sEPSCs recordings with a holding potential of −70 mV. The trace of sEPSC is shown in the box on the right. The above recording is the current obtained using the proposed method with a final seal resistance of 3.9 GΩ, while the below recording is the current obtained using the conventional method with a final seal resistance of 1.2 GΩ.

B. Electrophysiological Signal Recording Experiments

After the gigaseal resistance stabilized, negative pressure pulses were applied to break the cell membrane aspirated into micropipette, thereby establishing the whole-cell recording configuration. The experimental results in Fig. 7(a) show that the conventional method, the reported automated method, and the proposed method achieved successful whole-cell recording configurations for 6, 6, and 14 times, respectively. The higher success rate of whole-cell recording achieved by the proposed method is mainly attributable to the higher quality of the gigaseal.

The micropipette and target neuron during whole-cell configuration recording are shown in Fig. 8(a). Action potentials generated by the neuron in response to a 1000 ms-long current injection pulse at 100 pA are shown in Fig. 8(b). sEPSCs are electrical signals that result from the spontaneous release of neurotransmitters at excitatory synapses. Fig. 8(c) shows sEPSCs recorded from the neuron with the holding potential in the micropipette maintained at −70 mV. The above results prove limited negative influences of our method on neurons. The SNR is estimated using the sEPSC signal in according to the "Signal-to-noise Ratio Calculation" section in the "Supplemental file.docx". For sEPSCs of approximately 20 pA, the SNR of recordings using the proposed method is about 12 dB, which is 3 dB higher than the 9 dB achieved with the conventional method and 2 dB higher than the 10 dB achieved with the reported automated method. The higher SNR may be attributed to the higher seal resistance achieved by our method.

Long-time recordings of sEPSCs are important for studying synaptic transmission and plasticity [29]. Therefore, after

TABLE II
PERFORMANCE COMPARISON

indicator	conventional method [4]	automated method [12]	proposed method
gigaseal formation	55% (11/20)	60% (12/20)	85% (17/20)
gigaseal resistance	2.03±0.62 GΩ (n=11)	2.13±0.56 GΩ (n=12)	3.09±0.58 GΩ (n=17)
whole-cell recording	55% (6/11)	50% (6/12)	82% (14/17)
60-minute recording	33% (2/6)	33% (2/6)	57% (8/14)
SNR	9 dB	10 dB	12 dB

establishing the whole-cell recording configuration, sEPSCs were continuously recorded for 1 hour to monitor long-term synaptic activities. The experimental results shown in Fig. 7(a) demonstrate that, in 20 trials for each group, the conventional method, the reported automated method, and the proposed method achieved 2, 2, and 8 successful 1-hour sEPSC recordings, respectively. These results show that the proposed method achieves a fourfold increase in the number of long-time recordings, compared to both the conventional method and the reported automated method. The higher success rate of long-term recording may also be attributed to the formation of a tighter and more stable gigaseal achieved by our proposed method.

In the above experiments, key indicators for gigaseal formation tightness and stability, including gigaseal formation success rate, gigaseal resistance, whole-cell recording success rate, 60-minute recording success rate, and SNR, were compared among the proposed method, the conventional method, and the reported automated method [12], and the results are summarized in Table II.

C. Long-Time Glycine-Induced sEPSCs Recording Experiments

It has been reported that glycine plays an important role in activation of synaptic receptors [30], [31]. In an additional 5 long-time recordings using the proposed method, we studied the impact of glycine on the long-term induction of sEPSCs in CA1 hippocampal neurons. In each recording, the amplitudes and frequencies of sEPSCs were initially recorded 10 minutes before the application of glycine as a control group. Then the bath and perfusion solutions were replaced with aCSF containing 100 μM glycine, and the amplitudes and frequencies of sEPSCs were recorded for 60 minutes following the application of glycine (see Fig. 9(a)). The amplitudes and frequencies of sEPSC were normalized to the values from initial 10 minutes before the application of glycine. The whole 60-minute recording of Fig. 9(a) and the normalized values for each time period can be found in Fig. S5 and Table SI in the "Supplemental file.docx", respectively.

The results in Fig. 9(b)-(c) demonstrate that following the application of glycine for 15−60 minutes, both the amplitudes and frequencies of sEPSCs increased (with a normalized amplitude of 1.32±0.21 and a normalized frequency of 2.32±0.81 at 60 minutes, ∗p=0.014). This could be attributed partly to the activation of postsynaptic N-methyl-D-aspartate receptors (NMDARs) by glycine, which induces long-term potentiation (LTP) [30].

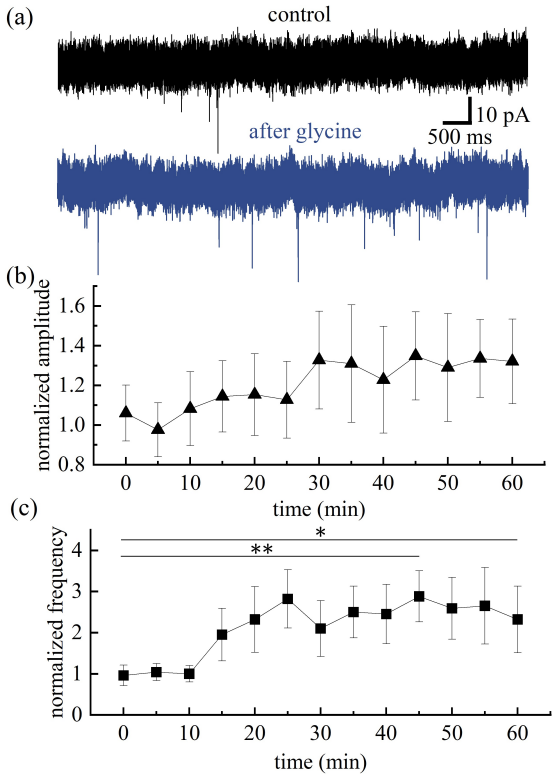

Fig. 9. Long-time sEPSC recordings before and after glycine application. (a) Current signals recorded before 10 minutes and after 60 minutes of glycine application (the downward peaks are sEPSCs). (b) Normalized sEPSC amplitude from 0 to 60 minutes after glycine application. (c) Normalized sEPSC frequency from 0 to 60 minutes after glycine application (0 minute, 0.96±0.25, 45 minute, 2.88±0.62, ∗p=0.008, 60 minute, 2.32±0.81, ∗p=0.014).

The above results demonstrate the effectiveness of our robotic patch clamp method in investigating the long-term variations of electrophysiological activities of neurons induced by drugs. This is of great meaning in research on pathological and pathogenic mechanisms of neuron system diseases and their potential treatments.

V. Discussion

Gigaseal formation is fundamental to the success rate and quality of patch clamp measurement. Our paper involves adjusting the pressure and voltage to generate a 3D driving force to promote gigaseal formation along a smooth, desired trajectory. Although this process may take longer than conventional manual method (approximately 30 s compared to 20 s), it results in a higher-quality gigaseal. Consequently, both the final seal resistance and success rate are superior to those achieved by conventional method. While our method adds a few seconds to the operation time, this slight increase in operation time is negligible in the context of the overall time required for whole-cell patch clamp recordings, which can last for tens of minutes [32]. Researchers prioritize the success rate

and quality of long-time whole-cell recording. This advantage significantly enhances the potential for broader applications of our method.

In this paper, the whole-cell patch clamp success rate of the proposed robotic method is significantly higher than that of the automated method proposed in [12] (70% vs. 30%). It is worth noting that the success rate of that automated method in this paper is lower than the reported success rates in [12] (64% and 37% in rodent visual and somatosensory cortices and human cortex, respectively). This is mainly because the success rate of the patch clamp method can be influenced by many factors, such as mouse age, brain region, incubation condition, room temperature, as well as the geometrical parameters of micropipette and the contact point and depth on cell surface. Even with the same gigaseal formation method, the success rate may vary across experiments conducted on different samples. Therefore, in our comparison of the conventional method, the previously reported automated method, and our proposed method, all experiments were conducted on pyramidal neurons in CA1 region in brain slices obtained from four-week-old mice under similar conditions. All the micropipette was pulled by a pipette puller with the same parameters and 4-7 MΩ bath resistance. The micropipette contact point was consistently chosen as the center of the ellipse-fitted cell contour, and the contact depth, estimated by the resistance increase, was consistently set to 0.5 MΩ above the bath resistance. The experimental comparison in this paper provides an objective evaluation of the advantages of our method.

It is worthy noting that there are still some limitations of this study. Although gigaseal formation is an essential step, the performance of patch clamp recordings can also be affected by many other factors. For example, before gigaseal formation, the micropipette tip is required to be sufficiently covered by the cell membrane to facilitate membrane aspiration into the micropipette. Therefore, the contact point selection between the micropipette opening and the 3D neuron surface is important because it can affect the contact angle between the micropipette opening and the cell surface, which further affects the covered area of micropipette opening by the cell membrane before membrane aspiration. In this paper, we used the conventional method of pressing the cell from its center point to make the micropipette tip covered by cell membrane. Analyzing the 3D morphology of the cell could help determine better contact points, thereby increasing the covered area of the micropipette opening by the membrane and further promoting gigaseal formation. In addition, after gigaseal formation, the conventional break-in method, which applies a large negative pressure pulse, is still used to rupture the membrane. This approach may disturb the seal between the membrane and the inner wall of the micropipette, thereby affecting its tightness and stability. Using other low-disturbance break-in methods, such as the perforated break-in technique, is expected to further improve the performance of patch clamp recordings. Moreover, there are still some control errors of resistance using our method. These errors may be attributed to the assumptions made in the modeling in Section III, such as the cylindrical shape assumption of the micropipette tip, the common black film assumption of the adhesion, and the solid wall assumption of the cell membrane. Although the designed adaptive controller can improve the performance of this system, the models can still be optimized in the future by investigating the effects of pressure and voltage on membrane creep under high-resolution microscopy. In this way, the control error of our method may be further improved in the future.

Gigaseal formation is an essential operational step in all patch clamp configurations, including cell-attached, whole-cell, inside-out, and outside-out configuration. In this paper, our proposed gigaseal formation method was applied to single-micropipette whole-cell patch clamp experiments on brain slices, which is the most popular patch clamp configurations due to its ability to measure the ion channels signals on the whole cell membrane. Since the method does not rely on visual guidance, it can be extended to all patch clamp configurations and applied to various cell types, including adherent cells, as well as in vivo systems such as blinded and labeled patch clamp. In vivo and multi-micropipette experiments will encounter more disturbances such as animal respiration, heartbeat, or the movement of other micropipettes, which have higher demands on the stability of gigaseal formation. In the future, the proposed robotic method and system can be specifically adapted to other patch clamp configurations and cell types. For example, in in vivo patch clamp systems, the micropipette resistance controller will need to be robust against disturbances caused by respiration and heartbeat on micropipette resistance. The proposed method will further validate its effectiveness in improving the success rate and quality of patch clamp recordings in more complex environments and under various disturbances.

The main contribution of this paper is improving the tightness and stability of gigaseal formation, thereby enhancing the recording success rate and precision, and extending the duration of patch clamp recordings. This improvement is expected to benefit a wide range of studies. For example, in behavioral studies on awake animals, even with head fixation, body movements, breaths and pulses in vessels can generate significant disturbances to patch clamp recordings, making a tight and stable gigaseal more essential for precise recordings of ion channel signals. In addition, in pharmacological studies on disease models, long-term patch clamp recordings are required to monitor the sustained and dynamic effects of drugs on cells, thereby extending the recording duration is therefore crucial. We have observed a long-term increase in the amplitude and frequency of sEPSCs in CA1 neurons following glycine application, which is similar to the results from reference [30], [31]. In the future, we will block potential glycine receptors to exclude their effect on sEPSCs and perform longer recordings using the proposed method to investigate the glycine-induced LTP. Although our method has not yet been applied to disease animal models, its higher success rate for long-time recordings and improved SNR are expected to enable its use in the future to study the pathogenesis, pathological mechanisms, and even drug screening for neurological diseases in disease mouse models.

VI. Conclusion

This paper presents a robotic precise patch clamp measurement method based on 3D-driven seal formation method to improve the measurement accuracy and duration of ion channel signals by providing a tight and stable gigaseal. First, the forces applied by aspiration pressure and voltage on the aspirated cell membrane inside the micropipette are analyzed, respectively. Then, a dynamic model of the gigaseal formation process driven by pressure and voltage is established to provide a 3D driving force on the target aspirated cell membrane. Further, a dual-input adaptive sliding mode controller is developed to form a tight and stable gigaseal to improve the measurement accuracy and duration in patch clamp operation. Finally, a robotic precise patch clamp measurement process was established based on the above work. Whole-cell patch clamp experiments on CA1 pyramidal neurons of mouse brain slices demonstrate that, in comparison to the current 2D-driven method, the proposed patch clamp measurement method has a significantly higher success rate in gigaseal formation (85% vs. 55% and 60%), higher final seal resistance (3.09 GΩ vs. 2.03 GΩ and 2.13 GΩ), and a fourfold increase in successful long-time recordings compared to both the conventional method and the reported automated method (8 vs. 2 and 2 successful 1-hour recordings in 20 trials), demonstrating a tighter and more stable gigaseal produced by our method. In sEPSC recordings, our method achieves a 3 dB higher SNR (12 dB vs. 9 dB). Based on long-time recordings using our method, long-term glycine-induced increases in amplitude (32%) and frequency (132%) of sEPSCs were detected. With above advantages, our method is expected to facilitate the research on pathological and pathogenic mechanisms of neuron system diseases and their potential treatments.

References

[1] E. Neher and B. Sakmann, "Single-channel currents recorded from membrane of denervated frog muscle fibres," *Nature*, vol. 260, no. 5554, pp. 799-802, 1976.

[2] D. Lovisolo, "Patch clamp: the first four decades of a technique that revolutionized electrophysiology and beyond," *Reviews of Physiology, Biochemistry and Pharmacology*, pp. 1-28, 2022.

[3] H. Shi, J. Shi, S. Tang, P. Yu, C. Su, and L. Liu, "Mechano-electrophysiological Signals Measuring System based on Cantilevered Micropipette Force Electric Sensor," *IEEE Transactions on Instrumentation and Measurement*, 2025.

[4] C. R. Cadwell et al., "Multimodal profiling of single-cell morphology, electrophysiology, and gene expression using Patch-seq," *Nature protocols*, vol. 12, no. 12, pp. 2531-2553, 2017.

[5] T. M. Suchyna, V. S. Markin, and F. Sachs, "Biophysics and structure of the patch and the gigaseal," *Biophysical journal*, vol. 97, no. 3, pp. 738-747, 2009.

[6] D. Das, A. Wong, T. N. Friedman, B. J. Kerr, H. T. Kurata, and S. M. Lamothe, "Reducing agents facilitate membrane patch seal integrity and longevity," *Channels*, vol. 18, no. 1, p. 2297621, 2024.

[7] A. Priel, Z. Gil, V. T. Moy, K. L. Magleby, and S. D. Silberberg, "Ionic requirements for membrane-glass adhesion and giga seal formation in patch-clamp recording," *Biophysical journal*, vol. 92, no. 11, pp. 3893-3900, 2007.

[8] C.-C. Chen et al., "Patch-clamp technique to characterize ion channels in enlarged individual endolysosomes," *Nature Protocols*, vol. 12, no. 8, pp. 1639-1658, 2017.

[9] T. Sordel et al., "The development of high quality seals for silicon patch-clamp chips," *Biomaterials*, vol. 31, no. 28, pp. 7398-7410, 2010.

[10] C. J. Milligan and L.-H. Jiang, "Automated planar patch-clamp recording of P2X receptors," in *Purinergic Signaling: Methods and Protocols:* Springer, 2019, pp. 285-300.

[11] S. B. Kodandaramaiah et al., "Multi-neuron intracellular recording in vivo via interacting autopatching robots," *Elife*, vol. 7, p. e24656, 2018.

[12] K. Koos et al., "Automatic deep learning-driven label-free image-guided patch clamp system," *Nature communications*, vol. 12, no. 1, pp. 1-11, 2021.

[13] L. A. Annecchino, A. R. Morris, C. S. Copeland, O. E. Agabi, P. Chadderton, and S. R. Schultz, "Robotic automation of in vivo two-photon targeted whole-cell patch-clamp electrophysiology," *Neuron*, vol. 95, no. 5, pp. 1048-1055. e3, 2017.

[14] Q. Zhao et al., "Robotic patch clamp based on noninvasive 3-D cell morphology measurement for higher success rate," *IEEE Transactions on Instrumentation and Measurement*, vol. 71, pp. 1-12, 2022.

[15] J. Qiu, Q. Zhao, R. Li, Y. Liu, B. Ma, and X. Zhao, "Robotic Fast Patch Clamp in Brain Slices Based on Stepwise Micropipette Navigation and Gigaseal Formation Control," *Sensors*, vol. 25, no. 4, p. 1128, 2025.

[16] Z. Gil, S. D. Silberberg, and K. L. Magleby, "Voltage-induced membrane displacement in patch pipettes activates mechanosensitive channels," *Proceedings of the National Academy of Sciences*, vol. 96, no. 25, pp. 14594-14599, 1999.

[17] M. Liu et al., "Robotic Improved Micropipette Aspiration Method for Accurate Measurement of Cellular Mechanical Properties," *IEEE Transactions on Instrumentation and Measurement*, vol. 74, pp. 1-8, 2025.

[18] T. Ursell, A. Agrawal, and R. Phillips, "Lipid bilayer mechanics in a pipette with glass-bilayer adhesion," *Biophysical journal*, vol. 101, no. 8, pp. 1913-1920, 2011.

[19] R. I. Slavchov, T. Nomura, B. Martinac, M. Sokabe, and F. Sachs, "Gigaseal mechanics: creep of the gigaseal under the action of pressure, adhesion, and voltage," *The Journal of Physical Chemistry B*, vol. 118, no. 44, pp. 12660-12672, 2014.

[20] J. Qiu et al., "Robotic Intracellular Pressure Measurement Based on Improved Balance Pressure Model," *IEEE Transactions on Instrumentation and Measurement*, vol. 73, pp. 1-9, 2024.

[21] D. Exerowa, A. Nikolov, and M. Zacharieva, "Common black and Newton film formation," *Journal of Colloid and Interface Science*, vol. 81, no. 2, pp. 419-429, 1981.

[22] A. Alizadeh, W. L. Hsu, M. Wang, and H. Daiguji, "Electroosmotic flow: From microfluidics to nanofluidics," *Electrophoresis*, vol. 42, no. 7-8, pp. 834-868, 2021.

[23] M. Chinappi, M. Yamaji, R. Kawano, and F. Cecconi, "Analytical model for particle capture in nanopores elucidates competition among electrophoresis, electroosmosis, and dielectrophoresis," *ACS nano*, vol. 14, no. 11, pp. 15816-15828, 2020.

[24] C. S. Drapaca, "An electromechanical model of neuronal dynamics using Hamilton's principle," *Frontiers in Cellular Neuroscience*, vol. 9, p. 271, 2015.

[25] P. Jonsson, J. P. Beech, J. O. Tegenfeldt, and F. Hook, "Mechanical behavior of a supported lipid bilayer under external shear forces," *Langmuir*, vol. 25, no. 11, pp. 6279-6286, 2009.

[26] S. F. Scagliusi et al., "Bioimpedance Spectroscopy-Based Edema Supervision Wearable System for Noninvasive Monitoring of Heart Failure," *IEEE Transactions on Instrumentation and Measurement*, vol. 72, pp. 1-8, 2023

[27] K. Li et al., "Neuron Contact Detection Based on Pipette Precise Positioning for Robotic Brain-Slice Patch Clamps," *Sensors*, vol. 23, no. 19, p. 8144, 2023. negative pressure pulses

[28] M. Murthy and G. Turner, "Whole-cell in vivo patch-clamp recordings in the Drosophila brain," *Cold Spring Harbor Protocols*, vol. 2013, no. 2, p. pdb. prot071704, 2013.

[29] T. Manabe, "Analysis of Synaptic Plasticity with the Slice Patch-Clamp Recording Technique," in *Patch Clamp Techniques: From Beginning to Advanced Protocols*, Y. Okada Ed. Tokyo: Springer Japan, 2012, pp. 147-157.

[30] W.-Y. Lu, H.-Y. Man, W. Ju, W. S. Trimble, J. F. MacDonald, and Y. T. Wang, "Activation of synaptic NMDA receptors induces membrane insertion of new AMPA receptors and LTP in cultured hippocampal neurons," *Neuron*, vol. 29, no. 1, pp. 243-254, 2001.

[31] L.-J. Li et al., "Glycine potentiates AMPA receptor function through metabotropic activation of GluN2A-containing NMDA receptors," *Frontiers in molecular neuroscience*, vol. 9, p. 102, 2016.

[32] D. Vandael, Y. Okamoto, C. Borges-Merjane, V. Vargas-Barroso, B. A. Suter, and P. Jonas, "Subcellular patch-clamp techniques for single-bouton stimulation and simultaneous pre-and postsynaptic recording at cortical synapses," *Nature Protocols*, vol. 16, no. 6, pp. 2947-2967, 2021.